Available online at www.sciencedirect.com
ScienceDirect
Trans. Nonferrous Met. Soc. China 24(2014) 2366−2373
Transactions of Nonferrous Metals Society of China
www.tnmsc.cn

Microstructures and mechanical properties of extruded 2024 aluminum alloy reinforced by $FeNiCrCoAl_3$ particles

Zhi-wei WANG[1], Yan-bo YUAN[1], Rui-xiao ZHENG[1], Kei AMEYAMA[2], Chao-li MA[1]

1. Key Laboratory of Aerospace Advanced Materials and Performance of Ministry of Education, School of Material Science and Engineering, Beihang University, Beijing 100191, China;
2. Department of Mechanical Engineering, Faculty of Science and Engineering, Ritsumeikan University, 1-1-1Nojihigashi, Kusatsu, Shiga 525-8577, Japan

Received 17 October 2013; accepted 30 April 2014

Abstract: Different proportions of commercial 2024 aluminum alloy powder and $FeNiCrCoAl_3$ high entropy alloy (HEA) powder were ball-milled (BM) for different time. The powder was consolidated by hot extrusion method. The microstructures of the milled powder and bulk alloy were examined by X-ray diffraction (XRD), scanning electron microscopy (SEM) and transmission electron microscopy (TEM). Mechanical properties of the extruded alloy were examined by mechanical testing machine. The results show that after BM, the particle size and microstructures of the mixed alloy powder change obviously. After 48 h BM, the average size of mixed powder is about 30 nm, and then after hot extrusion, the average size of grains reaches about 70 nm. The compressive strength of the extruded alloy reaches 710 MPa under certain conditions of milling time and composition. As a result of the identification of the nano-/micro-structure−property relationship of the samples, such high strength is attributed mainly to the nanocrystalline grains of α(Al) and nanoscaled $FeNiCrCoAl_3$ particles, and the fine secondary phase of Al_2Cu and Fe-rich phases.
Key words: aluminium alloys; $FeNiCrCoAl_3$ reinforced particles; high entropy alloy; ball milling; hot extrusion; nano-precipitates

1 Introduction

There is increasing interest in the development of highstrength light alloys because of the recent strong demands for mass reduction in transportation vehicles. Aluminum alloys are the most widely used light alloys for mass reduction in structural components.

Most of wrought aluminum alloys are strengthened by precipitation hardening, and the highest strength is ~600 MPa, reported for Al−Cu−Li based alloys [1]. However, further strengthening may be possible by grain attainable in wrought products. One way to achieve the nanocrystalline microstructure from aluminum-based alloy is the rapid solidification process. For example, Al−TM−RE amorphous-based alloys and their composites with nanocrystals were reported to have strengths more than 1 GPa [2−8]. The strength is really remarkable compared with conventional wrought alloys in the compression mode. For structural applications, it is essential to achieve such a high strength in bulk materials. Many attempts have been made to consolidate rapidly solidified powders or mechanically alloyed powders using hot extrusion [9−14]. And now, reinforced particles in Al matrix composites were almost used with hard metal powders, and inorganic non-metallic materials more. For examples, SASAKI et al [15] consolidated nanocrystalline Al−5%Fe (mole fraction) produced by mechanical alloying by spark plasma sintering. LI et al [16] researched the boundaries and interfaces in 5083Al/B_4C alloys. High entropy alloy (HEA) has been studied extensively in recent years, and has more excellent properties than conventional alloys: high ability of forming nano-scale precipitates, good thermal stability, superior extensive or compressive properties, extremely high hardness, excellent anticorrosive properties, special electrical and magnetic properties, and simple microstructures with solid solution of multiple elements. Great applications, such as molds and structural materials at high temperature, wearing and abrasion-

Foundation item: Project (2012CB619503) supported by the Nation Basic Research Program of China; Project (2013AA031001) supported by the National High Technology Research and Development Program of China; Project (2012DFA50630) supported by the International Science & Technology Cooperation Program of China
Corresponding author: Chao-li MA; Tel: +86-10-82339772; E-mail: machaoli@buaa.edu.cn
DOI: 10.1016/S1003-6326(14)63358-6

resistant coating, and even military weapons, have generally been expected in terms of the above unique characteristics. Consequently, not only large applied advantages but also great investigation potential indeed exist in HEAs. However, researches in HEAs as strengthening particles were rarely less. In this work, $FeNiCrCoAl_3$ high entropy alloy was used as strengthening particles in Al matrix composites. As the microstructure and property evolution were largely dependent on the mechanical alloying (MA) conditions such as MA time, process control agents (PCA) [17,18] and the amount of strengthening particles, these process parameters were varied to optimize the microstructure. In the case of 2024 aluminum alloy, hot extrusion breaks the typical oxide layer that coats the powder, providing better bonding of the particles.

The purposes of this work are to report the detailed processing conditions, mechanical properties and microstructure–property relationships of high- strength nanocrystalline Al alloys strengthened using $FeNiCrCoAl_3$ particles processed by a combination of MA and hot extrusion.

In this work, the application of innovative high-entropy alloy as aluminum reinforcing particles broadens the ranges of the particle reinforced aluminum matrix composite. For future aluminum powder metallurgy research methods, this work has great reference value.

2 Experimental

The powders of pure commercial 2024 aluminum alloy (99.5% in purity and 10−30 μm in diameter) and $FeNiCrCoAl_3$ (99.9% in purity and 10−100 μm in diameter), as raw materials, were prepared by Aerosol method, respectively. The related element contents of the commercial 2024 aluminum alloy powder are listed in Table 1.

Table 1 Element contents of 2024 aluminum alloy powder (mass fraction, %)

Al	Cu	Mg	Mn
92−95	3.7−4.2	1.2−1.5	0.15−0.8

The mixed powder of 2024 commercial aluminium alloy and $FeNiCrCoAl_3$ alloy was ball milled in a planetary high energy ball mill (Fritsch Pulverisette P−5) at room temperature using stainless steel vials and balls as milling media and alcohol as process control agent (PCA). The milling speed and ball-to-powder ratio were 300 r/min and 10:1, respectively. The powder was under the argon atmosphere to prevent powder oxidation. Variation in the particle size as a function of milling time was determined by Microtrac S3500 laser particle size analyzer and it was also verified by scanning electron microscopy (SEM) and electron probe microscopy (EPM). X-ray diffraction analysis (XRD) was carried out by RIGAKU RINT−2000 X-ray diffractometer, with Cu K_α radiation to determine the crystallite size and lattice strain as a function of ball-milling (BM) time. The nanocrystalline powder was consolidated by hot compression, and then by hot extrusion. The powder was extruded to fully dense bars of 7 mm in diameter and 5 mm in thickness by high strength heat-resistant stainless steel punches and dies. The vacuum hot extrusion (VHE) was carried out at 773 K (~60 K/min heating rate) for 10 min under the vacuum of 10^{-3} Pa. Uniaxial pressure was applied to the powder throughout the VHE cycle until the desired sintering temperature was attained, when the compression reached the maximum value of 500 MPa. Cylindrical samples of 4 mm in diameter and 8 mm in height (l/d ratio of 2) were cut from the VHE bar by electro discharge machine. All faces of the cylindrical compression samples were made parallel by polishing carefully. The compression tests were carried out by INSTRON 3367 machine. Compression rate was 0.2 mm/min, and the entrance force was 5 N. Microstructures of the mixed powder and VHE pellets were investigated by CamScan−3400 SEM and JEM−2100F TEM operating at 200 kV.

3 Results

3.1 Mechanically alloyed powders

The powders of pure commercial 2024 aluminum alloy (99.5% in purity and 10−30 μm in diameter) and $FeNiCrCoAl_3$ (99.9% in purity and 5−100 μm in diameter) are shown in Figs. 1(a) and (b), respectively. The average diameter of raw $FeNiCrCoAl_3$ particles is ~40 μm. After BM, the mixed powder has irregular shape, as shown in Figs. 1(c) and (d). This is because the sphere particles of starting powder are squashed and fractured by the fragmentation of fragile flakes and/or by a fatigue failure mechanism with collision of steel spheres. Then the lamellar structure fragments are bonded by cold welding which is a kind of strong agglomerating force.

A comparison between these two profiles shows that the MA causes peak broadening due to the grain refinement and straining, and the peak shift to higher angles indicates the dissolution of Cu or Mg atoms into the α(Al) phase. Figure 2 shows the XRD patterns of initial 2024 powder and the powder milled. The diffraction patterns show small broadening and lowing of Al peaks after milling, which may be the result of the deformation induced by the processing and the grain refining and straining, as can be got from the Scherrer formula as follows:

$$d = \frac{0.9\lambda}{B\cos\theta} \quad (1)$$

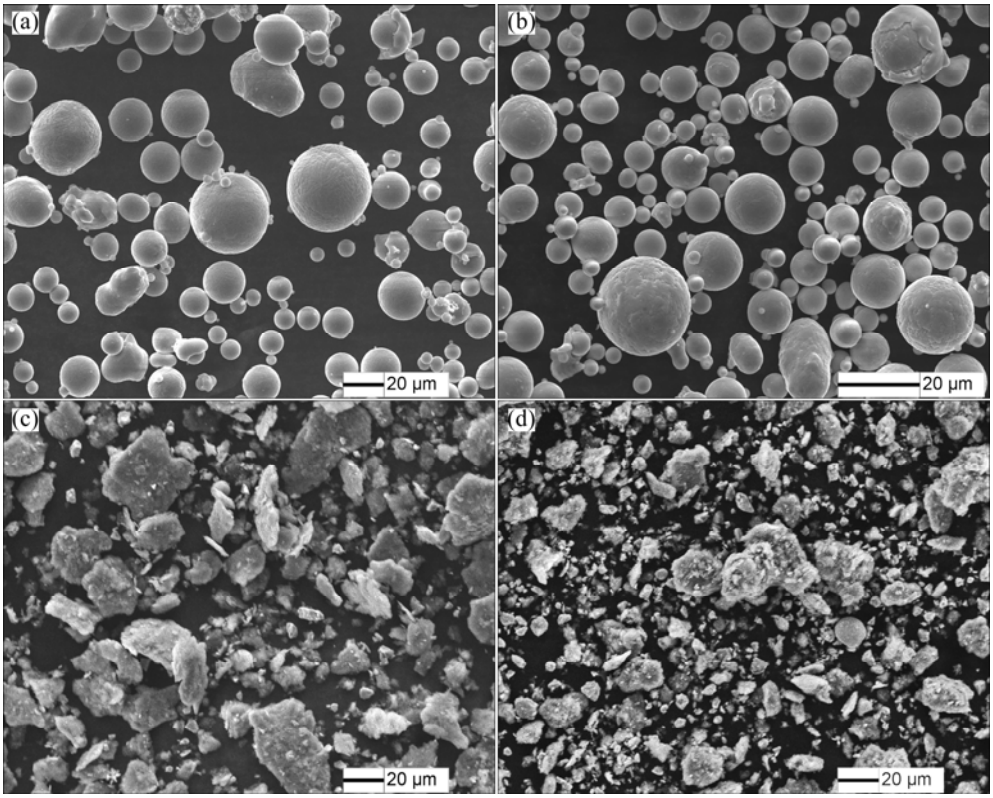

Fig. 1 SEM images of pure commercial 2024 aluminum powder (a), pure $FeNiCrCoAl_3$ alloy powder (b) and 20% $FeNiCrCoAl_3$+ 80% 2024 alloy powder after 24 h BM (c) and 48 h BM (d)

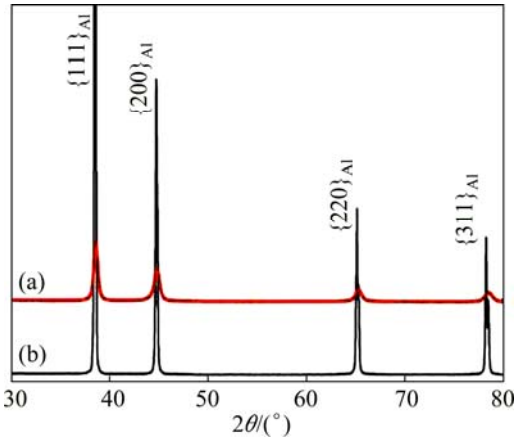

Fig. 2 XRD patterns of commercial 2024 Al alloy powder: (a) With BM for 48 h; (b) Without BM

where d is the crystallite size; λ is the wavelength of the X-radiation used; B is the peak width at half the maximum intensity; θ is the Bragg angle [17].

Figure 3(a) shows the XRD patterns of pure $FeNiCrCoAl_3$ powder. And the microstructure of $FeNiCrCoAl_3$ is composed of single BCC phase, Al is the BCC former. This conclusion conforms to the same results of Refs. [19−21]. While in Fig. 3(b), the 2024 aluminum alloy powder is composed single FCC phase. Compared with Figs. 3(a) and (b), after ball milling for 48 h, as shown in Fig. 3(c), the X-ray diffraction peaks are very low, no more than 2000 cps, and the structures are typical of FCC in aluminium matrix and BCC in Fe based strengthening particles. Just like that mentioned above, MA causes peak broadening due to the grain refinement and straining, and the peak shift to higher angles indicates the dissolution of atoms into the α(Al) phase and/or the Fe based strengthening particles.

The bright and dark field TEM images of the powder of MA alloy after 48 h BM are shown in Figs. 4(a) and (b). Figure 4(c) shows the dark field TEM image of the powder of the same sample after 24 h BM. The dark field TEM image shows the {111} reflection of the α(Al) in Figs. 4(b) and (c). Aluminum nanocrystals are shown in Figs. 4(b) and (c), and the average diameter in Fig. 4(b) is about 20 nm, while the average diameter in Fig. 4(c) is about 50 nm. As BM time increases, the grain sizes decrease [15].

3.2 Compressive behavior of hot extruded samples

Figure 5 shows the room temperature compressive engineering stress–strain curves of the hot extruded samples. Line (a) is the curve of hot extruded 2024 aluminum alloy produced from the powders mechanically alloyed for 48 h BM with a fixed amount of PCA (4%). The sintering conditions for all the samples are the same, as shown in Fig. 5. The room

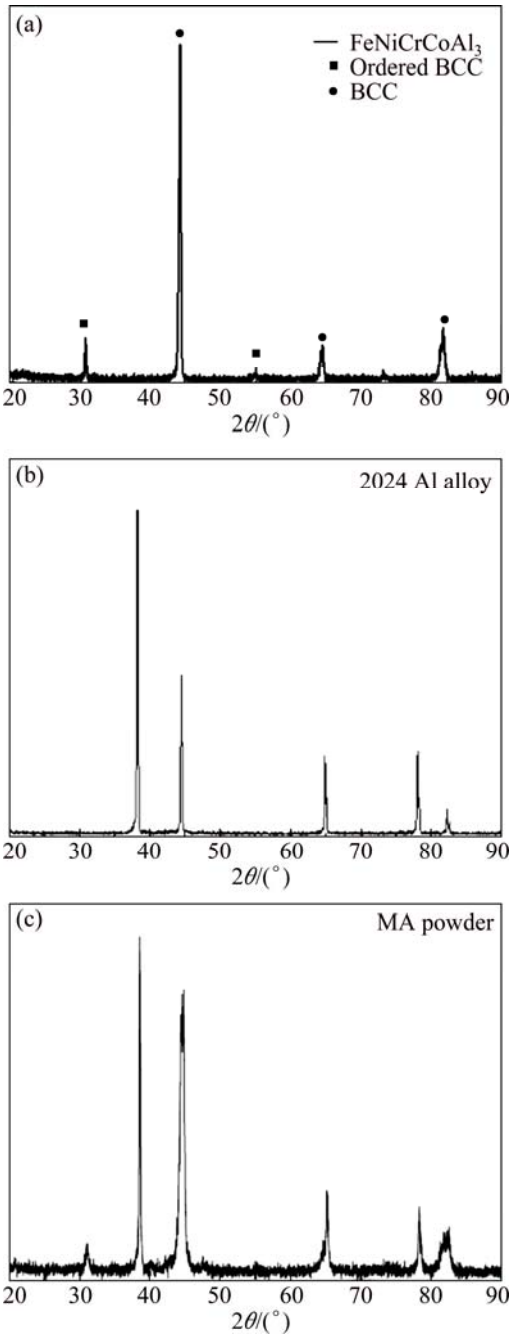

Fig. 3 XRD patterns of $FeNiCrCoAl_3$ powder (a), 2024 aluminum alloy powder (b) and mechanical alloy after 48 h BM (c)

temperature strengths of the samples increase with MA time. After 48 h BM, the compressive strength of pure 2024 Al sintering sample is nearly twice that of non-BM sample, reaching about 500 MPa. BM can refine grains, and increase dissolution of Cu or Mg atoms into the α(Al) phase. During hot extrusion, the Al_2Cu phase is precipitated from supersaturated aluminum matrix. Line (d) is curve of 40% (mass fraction) $FeNiCrCoAl_3$ alloy in 2024 aluminum matrix after 48 h BM, and its compressive strength is about 500 MPa. While 20% or 30% raw 2024 aluminum alloy powder is added in 40%

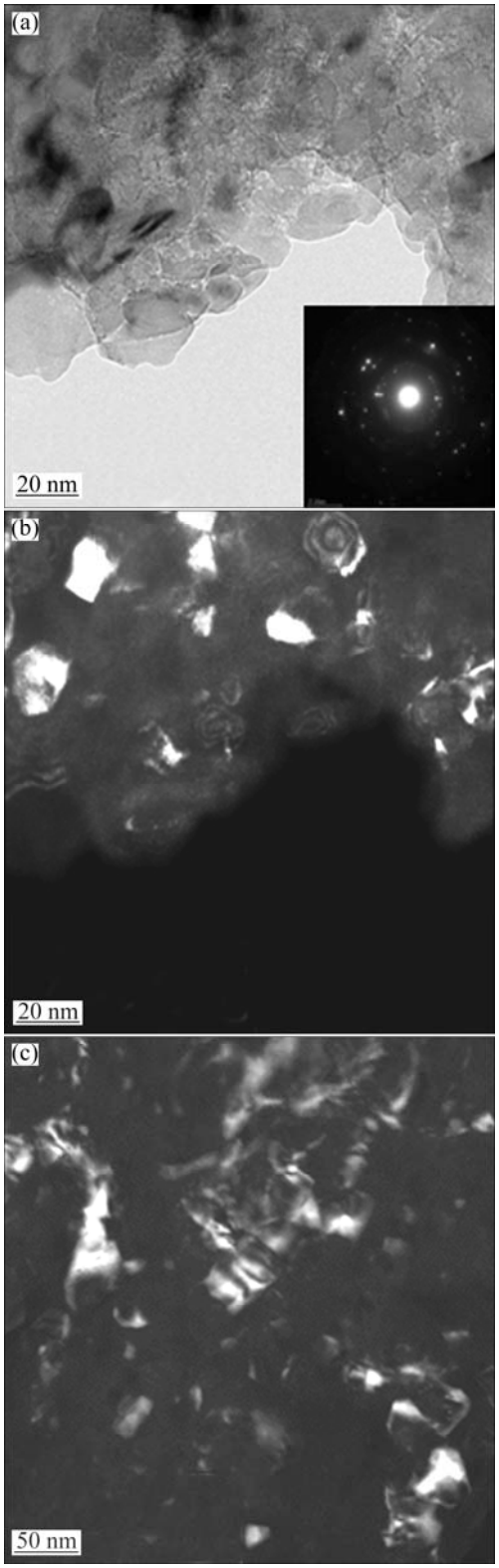

Fig. 4 Bright (a) and dark field (b) TEM images of {111} reflection of α(Al) of MA powder after 48 h BM and SAD pattern taken from nanocrystalline region of MA powder after 24 h (c)

$FeNiCrCoAl_3$ alloy in 2024 aluminum matrix with other conditions the same, the compressive strength increases by 100 or 200 MPa. In particular, the strength of the

samples with addition of 30% raw aluminium alloy powder after hot extrusion in the same conditions reaches 710 MPa. When $FeNiCrCoAl_3$ is added, the ductility of sintering samples decreases obviously.

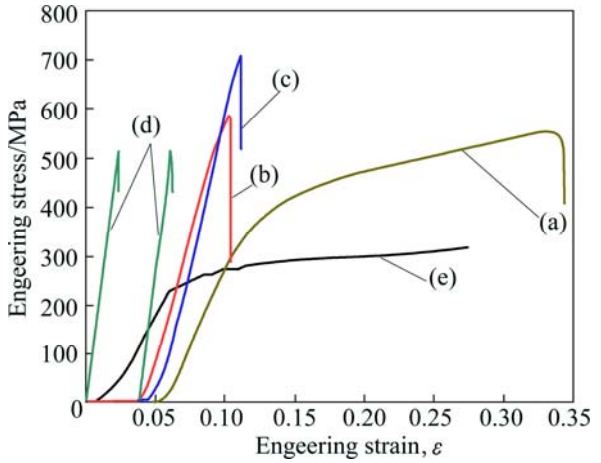

Fig. 5 Compressive stress−strain curves of extruded sample: (a) 2024 Al, BM 48 h; (b) 20% raw 2024 Al + 80% MA powder of 40% $FeNiCrCoAl_3$ alloy in 2024 Al matrix; (c) 30% raw 2024 Al + 70% MA powder of 40% $FeNiCrCoAl_3$ alloy in 2024 Al matrix; (d) 40% $FeNiCrCoAl_3$ alloy in 2024 Al matrix after 48 h BM; (e) Pure 2024 Al after 500 °C hot press and 500 °C hot extrusion

3.3 Microstructure of hot extruded samples

Figure 6 shows the XRD pattern of the sintered sample after 48 h BM with 4% PCA. The sample mainly consists of Al_2Cu, Al_6Fe and Al_3Fe phases. Figure 7 shows a backscattered electron EPMA image of 30% raw 2024 Al+70% MA powder of 40% $FeNiCrCoAl_3$ alloy in 2024 aluminium matrix. The black region is supposed to be α(Al) phase, as only Al could be detected by EDS analysis. The diffraction spots from 2024 aluminum matrix are confirmed to be Al_2Cu phase. The white bulk phases and white spots are $FeNiCrCoAl_3$ strengthening

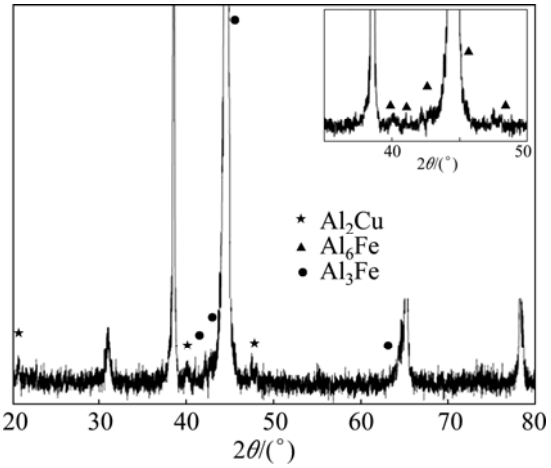

Fig. 6 XRD patterns of sintered 40% $FeNiCrCoAl_3$/2024 Al sample after 500 °C hot extrusion

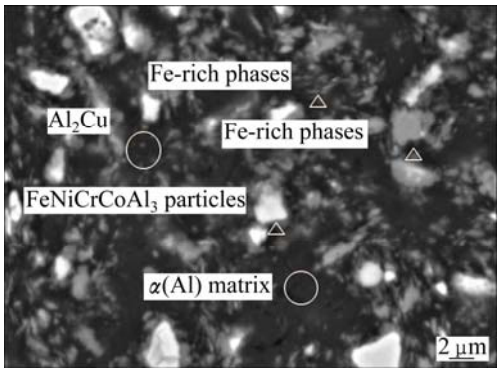

Fig. 7 BEI image of 30% raw 2024 Al+70% MA powder of 40% $FeNiCrCoAl_3$ alloy in 2024 Al matrix after 500 °C hot extrusion from EPMA

particles. The angular shaped needle-like and lath-like regions are Al_3Fe phases, the intermetallic compounds originating from the reaction of the Al-rich region and the $FeNiCrCoAl_3$ region. Multiple structures are formed in 30% raw 2024 Al + 70% MA powder of 40% $FeNiCrCoAl_3$ alloy in 2024 Al matrix, and the cracked $FeNiCrCoAl_3$ alloy particles are the core. After MA, the Fe and Cr atoms transit to Al matrix, and Al atoms transit to the strengthening particles. The outer coating is the coarse 2024 aluminum matrix.

Figure 8(a) shows a bright field TEM image of the sintered sample after 48 h MA with 4% PCA. The microstructure is composed of a randomly oriented nanocrystalline grain region and grain size is about 100 nm, as shown in Fig. 8(c). The diffraction spots from the Al_6Fe phase are confirmed in addition to the diffraction rings from α(Al) in the SAD pattern taken from the nanocrystalline region in Fig. 8(b). Figure 8(d) shows a dark-field TEM image using the {311} reflection of the Al_6Fe phase. The Al_6Fe phase is homogeneously dispersed within the nanocrystalline grain region as fine grains, and the grain size is ~40 nm. Figure 9(a) shows another bright field TEM image of the same sample. These are typical of nano Fe based strengthening grains, as shown in the SAD pattern. Figure 9(b) shows Al_2Cu grains in α(Al) matrix, and grain size is nearly 20 nm. Figures 9(c) and (d) show that the $FeNiCrCoAl_3$ strengthening particles are of typically BCC structure, as shown in Fig. 3(a).

4 Discussion

Figure 2 and Figs. 4(b) and (c) show that as MA time increases, grains size is continually refined. According to the Hall−Petch formula, the grains are refined, resulting in the value of d decreasing, the strength increasing and also ductility improving. The strength of the sintered sample increases with the MA time, as shown in Fig. 5 (lines (a) and (e)). In Fig. 5, the

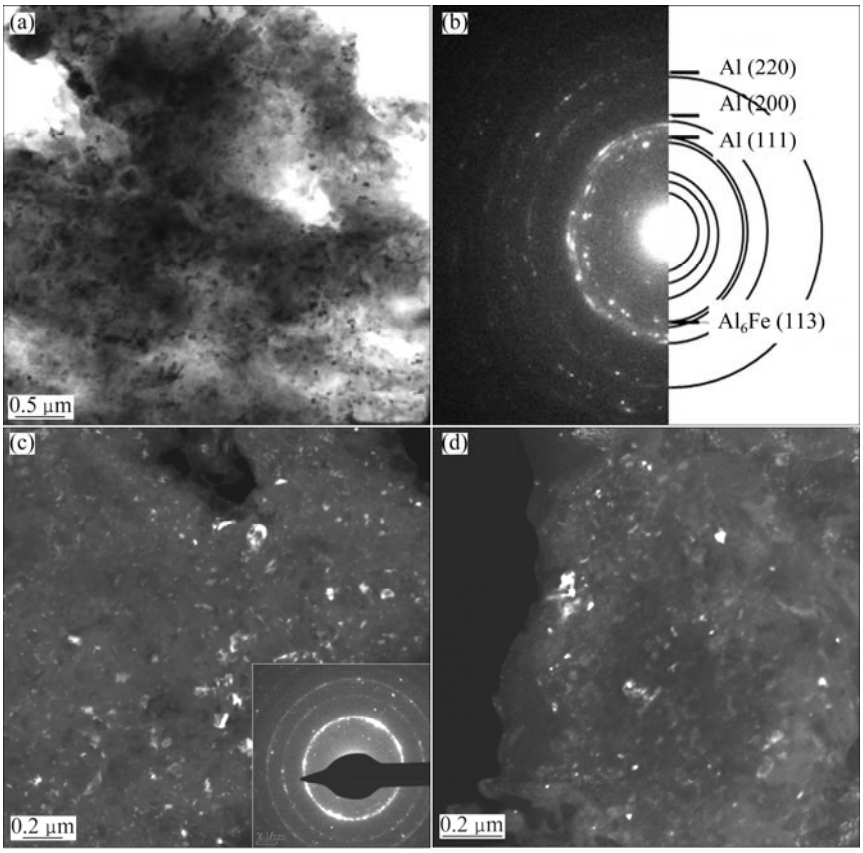

Fig. 8 Bright field TEM image (a), SAED pattern (b), and corresponding dark field TEM images using {111} of α(Al) (c) and {311} reflections of Al_6Fe phase (d)

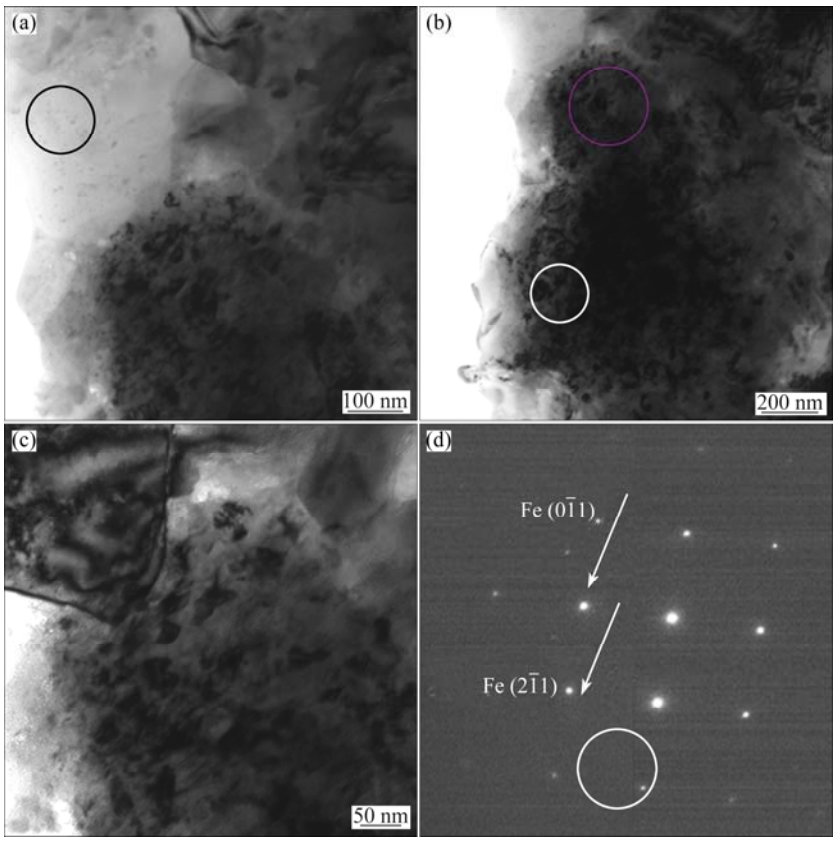

Fig. 9 Bright field TEM images of nanocrystalline region (a), aluminum matrix (b) and interface between strengthening particle and nanocrystalline region (c) and corresponding SAED pattern (d) in Fig. 9(c)

compressive strength of the hot extruded samples added with $FeNiCrCoAl_3$ strengthening particles (lines (b), (c), (d)) are higher than those of non-adding ones. The compressive strength of sample (line (c)) reaches 710 MPa, twice than that of non-BM pure 2024 Al alloy after sintering. Microstructure characterizations show that after MA, the grains are refined, and the fine nanocrystals, such as nano α(Al) grains, nano $FeNiCrCoAl_3$ grains and nano Al_6Fe grains, as shown in Figs. 8(c), (d) and Fig. 9(a), are dispersed in aluminum matrix. During hot extrusion, the diffusion of elements between $FeNiCrCoAl_3$ strengthening particles and 2024 aluminum matrix partly forms the Fe-rich secondary phases (Al_3Fe and Al_6Fe), and the other part of the diffusion elements in aluminum lattice forms solid solution strengthening. Nanoscale Al_2Cu phase is precipitated from the aluminum matrix. In Al matrix, Al_3Fe phase is hard and brittle [22]. The fine needle-like Al_3Fe phase is helpful to reinforcing the aluminum alloy, as shown in Fig. 7. These nanoscale crystals are helpful to hindering the movement of dislocations. As shown above, the compressive strength of the sintered samples with the reinforcing particles is obviously higher than that of non-adding ones.

Figure 5 shows that the compressive strength of the sintered sample of 40% $FeNiCrCoAl_3$ alloy in 2024 aluminum matrix after 48 h BM is almost equal to that of the 48 h BM pure aluminum samples after sintering, and its ductility deteriorates sharply. Microstructures reveal that bulk Al_3Fe phases are found in Fig. 7. Bulk Al_3Fe regions are considered as the source of cracks, as referred in Ref. [22]. It is the principal reason of deterioration of the ductility. This also explains that when raw 20% or 30% 2024 aluminum alloy powder is added in above sample powder, the strength increases obviously, as shown in Fig. 5 (lines (b) and (c)).

5 Conclusions

1) MA is helpful to refining grains. Bulk nanocrystalline Al multiple structure fabricated by MA and hot extrusion exhibits high compression strength, about 710 MPa at room temperature.

2) As a result of the identification of the nano-/micro-structure–property relationship of the various samples, such high strength is attributed mainly to the nanocrystalline grains of α(Al) and nanoscaled $FeNiCrCoAl_3$ particles, and the fine secondary phase of Al_2Cu and Fe-rich phases.

References

[1] POLMEAR I J. Light alloys [M]. Oxford: Butterworth-Heinemann, 2006: 97−204.

[2] KIM Y H, INOUE A, MASUMOTO T. Ultrahigh tensile strengths of Al88Y2Ni9M1 (M=Mn or Fe), amorphous alloys containing finely dispersed fcc Al particles [J]. Mater Trans JIM, 1990, 31(8): 747−749.

[3] LIU Bing, PENG Chao-qun, WANG Ri-chu, WANG Xiao-feng, LI Ting-ting. Recent development and prospects for giant plane aluminum alloys [J]. The Chinese Journal of Nonferrous Metals, 2010, 20(9): 1706−1713. (in Chinese)

[4] CHEN Song-yi, CHEN Kang-hua, JIA Le, PENG Guo-sheng. Effect of hot deformation conditions on grain structure and properties of 7085 aluminum alloy [J]. Transactions of Nonferrous Metals Society of China, 2013, 23(2): 329−334.

[5] HANSANG K, MEHDI E, KENTA T, TAKAMICHI M, AKIRA K. Combination of hot extrusion and spark plasma sintering for producing carbon nanotube reinforced aluminium [J]. Carbon, 2009, 47(3): 570−577.

[6] KAWAMURA Y, INOUE A, MASUMOTO T. Mechanical properties of bulk amorphous alloy compacts prepared by a closed processing system [J]. Scripta Metallurgica et Materialia, 1993, 29(1): 25−30.

[7] KAWAMURA Y, INOUE A, SASAMORI K, KATOH A, MASUMOTO T. Rapidly solidified powder metallurgy $Mg_{97}Zn_1Y_2$ alloys with excellent tensile yield strength above 600 MPa [J]. Mater Trans JIM, 1993, 42(7): 1172−1176.

[8] KIMURA H M, SASAMORI K, INOUE A. Formation and properties of Zr-based bulk quasicrystalline alloys with high strength and good ductility [J]. J Mater Res, 2000, 15(10): 2195−2208.

[9] SENKOV O N, MIRACLE D B, SCOTT J M, SENKOVA S V. Equal channel angular extrusion compaction of semi-amorphous $Al_{85}Ni_{10}Y_{2.5}La_{2.5}$ alloy powder [J]. J Alloys Comp, 2004, 1(2): 126−133.

[10] VARYUKHIN V N, TKATCH V I, MASLOV V V, BEYGELZIMER Y Y, SYNKOV S G, NOSENKO V K. Nanostructured $Al_{86}Gd_6Ni_6Co_2$ bulk alloy produced by twist extrusion of amorphous melt-spun ribbons [J]. Mater Sci and Eng A, 2006, 5(6): 172−177.

[11] NOH S J, JUNG T K, LEE D S, KIM M S. Microstructure and compressive behavior of Al-base amorphous/nanocrystalline alloys fabricated by powder forging mater [J]. Sci Eng A, 2007, 449−451: 799−803.

[12] WITKIN D B, LAVERNIA E J. Synthesis and mechanical behavior of nanostructured materials via cryomilling [J]. Prog Mater Sci, 2006, 51(1): 1−60.

[13] HAYES R W, RODRIGUEZ R, LAVERNIA E J. The mechanical behavior of a cryomilled Al−10Ti−2Cu alloy [J]. Acta Mater, 2001, 49(19): 4055−4068.

[14] SHAW L, LUO H, VILLEGAS J, MIRACLE D. Compressive behavior of an extruded nanocrystalline Al−Fe−Cr−Ti alloy [J]. Scripta Mater, 2004, 50(7): 921−925.

[15] SASAKI T T, OHKUBO T, HONO K, Microstructure and mechanical properties of bulk nanocrystalline Al−Fe alloy processed by mechanical alloying and spark plasma sintering [J]. Acta Materialia, 2009, 57: 3529−3538.

[16] LI Y, ZHANG Z, VOGT R, SCHOENUNG J M, LAVERNIA E J. Boundaries and interfaces in ultrafine grain composites [J]. Acta Materialia, 2011, 59: 7206−7218.

[17] SURYANARAYANA C. Mechanical alloying and milling [J]. Prog Mater Sci, 2001, 46(1−2): 1−184.

[18] SHAW L, ZAWARAH M, VILLEGAS J, LUO H, MIRACLE D. Thermal stability of nanostructured $Al_{93}Fe_3Cr_2Ti_2$ alloys prepared via mechanical alloying[J]. Metall Mater Trans A, 2003, 34: 159−163.

[19] TONG C J, CHEN Y L, CHEN S K, YEH J W, SHUN T T, TSAU C H, LIN S J S Y, CHANG S Y. Mechanical performance of the $Al_xCoCrCuFeNi$ high-entropy alloy system with multiprincipal elements Metal [J]. Mater Trans A, 2005, 36: 881−893.

[20] KAO Yih-farn, CHEN Ting-Jie, CHEN Swe-kai, YEH Jien-wei, Microstructure and mechanical property of as-cast, -homogenized, and -deformed $Al_xCoCrFeNi$ ($0\leq x\leq 2$) high-entropy alloys [J]. Journal of Alloys and Compounds, 2009, 488: 57−64.

[21] LEE C P, CHANG C C, CHEN Y Y, YEH J W, SHIH H C, Effect of the aluminium content of $Al_xCrFe1.5MnNi0.5$ high-entropy alloys on the corrosion behaviour in aqueous environments [J]. Corros Sci, 2008, 50: 2053−2060.

[22] ZHOU Zhen-ping, LI Rong-de, MA Jian-chao, WANG Yi. Effect of Ca on the morphology and distribution of iron-rich phase of hypereutectic Al−5%Fe alloy [J]. Foundry, 2004(2): 15−20. (in Chinese)

$FeNiCrCoAl_3$ 颗粒增强 2024 铝合基复合材料的显微组织和力学性能

王志伟[1]，原燕波[1]，郑瑞晓[1]，Kei AMEYAMA[2]，马朝利[1]

1. 北京航空航天大学 材料科学与工程学院 空天先进材料与服役教育部重点实验室，北京 100191；
2. Department of Mechanical Engineering, Faculty of Science and Engineering, Ritsumeikan University, 1-1-1Nojihigashi, Kusatsu, Shiga 525-8577, Japan

摘 要：将不同比例的 2024 商业铝粉和由气雾化法制得的 $FeNiCrCoAl_3$ 高熵合金粉球磨不同时间，然后，将混合粉末通过热挤出方法成型。通过 XRD、SEM 和 TEM 方法研究球磨粉和烧结后合金的显微组织，并通过应力测试机测试挤出样品的力学性能。结果表明：球磨后，粉末的晶粒尺寸减小，显微组织发生变化。混合粉末经过 48 h 球磨后，颗粒平均直径约为 30 nm；粉末在热挤出后，晶粒尺寸约为 70 nm。在适当条件下，热挤出合金的压缩强度达到 710 MPa。通过对样品组织和性能关系的分析发现：强度的增加主要归因于纳米 α(Al)和 $FeNiCrCoAl_3$ 颗粒以及析出的超细二次相 Al_6Fe 相和富 Fe 相。

关键词：铝合金；$FeNiCrCoAl_3$ 增强颗粒；高熵合金；球磨；纳米析出相

(Edited by Chao WANG)